JCTC Journal of Chemical Theory and Computation

Article

pubs.acs.org/JCTC

Rapid Sampling of Folding Equilibria of β-Peptides in Methanol Using a Supramolecular Solvent Model

Wei Huang, Sereina Riniker, and Wilfred F. van Gunsteren*

Laboratory of Physical Chemistry, Swiss Federal Institute of Technology, ETH, 8093 Zürich, Switzerland

Supporting Information

ABSTRACT: Molecular dynamics simulation of biomolecules in solvent using an atomic model for both the biomolecules and the solvent molecules is still computationally rather demanding considering the time scale of the biomolecular motions. The use of a supramolecular coarse-grained (CG) model can speed up the simulation considerably, but it also reduces the accuracy inevitably. Combining an atomic fine-grained (FG) level of modeling for the biomolecules and a supramolecular CG level for the solvent into a hybrid system, the increased computational efficiency may outweigh the loss of accuracy with respect to the biomolecular properties in the hybrid FG/CG simulation. Here, a previously published CG methanol model is reparametrized, and then a 1:1 mixture of FG and CG methanol is used to calibrate the FG-CG interactions using thermodynamic and dielectric screening data for liquid methanol. The FG-CG interaction parameter set is applied in hybrid FG/CG solute/solvent simulations of the folding equilibria of three β-peptides that adopt different folds. The properties of the peptides are compared with those obtained in FG solvent simulations and with experimental NMR data. The comparison shows that the folding equilibria in the pure CG solvent simulations are different from those in the FG solvent simulations because of the lack of hydrogen-bonding partners in the supramolecular CG solvent. Next, we introduced an FG methanol layer around the peptides in CG solvent to recover the hydrogen-bonding pattern of the FG solvent simulations. The result shows that with the FG methanol layer, the folding equilibria of the three β-peptides are very similar to those in the FG solvent simulations, while the computational efficiency is at least 3 times higher and the cutoff radius for nonbonded interactions could be increased from 1.4 to 2.0 nm.

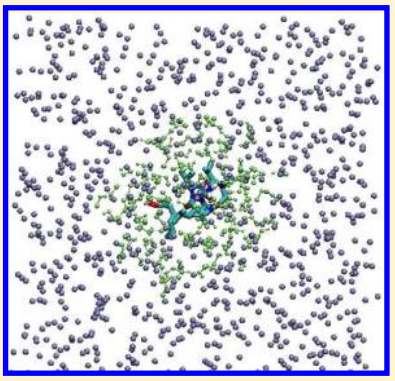

1. INTRODUCTION

Molecular dynamics (MD) simulation of biomolecular systems at the atomic level is currently possible for systems of nanometer size containing up to 10^6 particles covering time periods of up to microseconds due to the increase of computer power.[1] Since many biomolecular processes occur on larger time scales, atomic-level MD simulation is not fast enough to study such processes. The use of supra-atomic or supramolecular coarse-grained (CG) models can speed up a simulation considerably, but it also inevitably reduces its accuracy. In biomolecules such as proteins or peptides, small changes in atomic detail may lead to large conformational changes, and as solutes, they present only a small part of the system to be simulated, while the solvent accounts for the vast majority of the computational cost and the details of the solvent-solvent interactions are of less importance to the property or biomolecular process to be investigated. Thus, the combination of atomic level of modeling for the solute and a supramolecular CG level for the solvent into a hybrid system may strike a proper balance between the simulation accuracy and speed by reducing the computational cost of the simulation and retaining the details of the region of interest, i.e. the biomolecule, simultaneously.[2] Simple, efficient, polarizable supramolecular CG models for different solvents, such as water, dimethyl sulfoxide, chloroform, and methanol, have been developed recently[3,4] and are compatible with an atomic-level force field such as GROMOS[5,6] for the solute. Two to five atomic-level fine-grained (FG) solvent molecules are subsumed into a single CG bead containing two interaction sites which carry opposite charges and represent a polarizable dipole.

The challenge of developing a model that spans FG/CG levels of modeling is to find a physically correct balance between the three types of interactions present in such a system: interactions between FG particles (FG-FG), interactions between FG and CG particles (FG-CG), and interactions between CG particles (CG-CG).[2] A variety of ways to handle hybrid FG/CG systems has been proposed.[7−38] Recently, a relatively simple procedure employing a minimal reparametrization of the FG-CG interactions while leaving FG-FG and CG-CG interactions untouched was proposed by Riniker et al.[38] This hybrid FG/CG interaction representation has been tested in mixed-grained MD simulations of four proteins, and the results showed that the folds of the atomistic proteins in CG water are stable,[39] and a variety of structural properties matched those from purely FG simulations and experiment.[40] A next challenge is to reproduce the folding equilibrium of polypeptides solvated in a CG solvent.

The folding equilibria of β-peptides in methanol using an atomic-level methanol model have been investigated using

Received: January 21, 2014
Published: May 12, 2014

 © 2014 American Chemical Society

Table 1. Comparison of the Density ρ, Intercluster or Interbead Potential Energy V^{pot}, and Its Lennard-Jones and Coulomb Plus Reaction Field Components V^{LJ} and V^{CRF}, Average Dipole Moment $\langle\vec{\mu}\rangle$, Relative Static Dielectric Permittivity $\varepsilon(0)$, Surface Tension γ, and Self-Diffusion Coefficient D Measured Experimentally and Calculated from Simulations Using the FG and the Two Different CG Models of Methanol[c]

	ρ (g cm^{-3})	V^{pot} (kJ mol^{-1})	V^{LJ} (kJ mol^{-1})	V^{CRF} (kJ mol^{-1})	$\langle\vec{\mu}\rangle$ (D)	$\varepsilon(0)$	γ (mN m^{-1})	D (10^{-5} cm^2 s^{-1})
Exp.[a]	0.787				1.7	32.6	22.1	2.4
FG[b]	0.786				2.29	19.8	21.9	2.4
FG_{cl}		−21	−7	−14	5.40			1.0
CG_{old}	0.787	−14	−10	−5	5.49	25.4	21.3	10.9
CG_{new}	0.784	−17	−6	−11	5.48	26.8	18.0	11.6

[a]From ref 64 other than D, which is from ref 66. [b]From ref 59 other than γ, which is from ref 4. [c]All experimental and simulated values correspond to 298 K and 1 atm unless specified otherwise. Note that the values given in the first line of the FG data are for individual FG molecules, whereas the second line, labeled FG_{cl} gives values for clusters of FG molecules and are meant for comparison to the CG value. CG_{old} denotes the original CG methanol model from ref 4, and CG_{new} denotes the reparametrized CG methanol model used in our work.

different GROMOS force-field parameter sets.[41−46] Here, we employ a reparametrized polarizable supramolecular CG model of methanol[4] to speed-up the simulations of three different β-peptides that adopt different dominant folds (L-helix, R+L helices, hairpin) and compare their folding equilibria in hybrid FG/CG (solute/solvent) simulations with those obtained in purely FG simulations as well as with experimental data. The hybrid FG/CG scheme used in this work is based on the one developed by Riniker et al.[38−40] A proper parametrization of the FG-CG interactions is investigated using a 1:1 mixture of FG/CG methanol, for which a few FG/CG interaction parameters are varied to reproduce the properties of pure methanol as obtained from experiment or simulation using an FG model. One parameter set is selected from these simulations of the liquid state of methanol and subsequently used in simulating three β-peptides solvated in pure CG methanol (called CG simulations) or with a FG methanol layer surrounding the peptides in CG methanol (named FG_layer simulations) using these FG/CG parameters. The properties of the peptides are compared with those obtained in pure FG methanol (FG simulations) and with experimental NMR data.

2. METHODS

2.1. Fine-Grained and Coarse-Grained Models of Methanol. The united-atom FG methanol model used for the FG simulations and for a mixture of FG and CG methanol is the simple rigid three-site model that is part of the GROMOS 53A6[47] and 54A7[6] force fields. In the CG model of methanol, four methanol molecules are subsumed into a single CG bead, which consists of two interaction sites or particles, the center of methanol particle (CM) and a dipole particle (DM). The two sites have a mass and carry opposite charges. They are connected by an unconstrained bond with an attractive quartic potential energy function, making the model polarizable. This CG model of methanol is described in detail in ref 4. The CM site interacts with the CM sites of other CG beads through a pairwise Lennard-Jones and an electrostatic potential energy function. The DM site interacts with both the CM and DM sites of other CG beads purely electrostatically. When trying to reproduce the properties of the CG methanol model of ref 4 we noticed an inconsistency between the values reported for the Lennard-Jones energy V^{LJ} and the electrostatic energy V^{CRF} of the FG clusters in the prelast line of Table II and the right panel of Figure 3. The correct values are $V^{LJ}(FG_{cl}) = -7$ kJ mol^{-1} and $V^{CRF}(FG_{cl}) = -14$ kJ mol^{-1}. This error in Table II of ref 4 implies that the CG model of ref 4 has a different distribution of the potential energy over V^{LJ} and V^{CRF} than the FG model, which makes this CG model less suitable for FG/CG simulations. So it was decided to reparametrize the CG methanol model of ref 4. The charge of the CM particle is changed from[4] −0.56 e to −0.53 e, and the charge of the DM particle is correspondingly changed from[4] 0.56 e to 0.53 e. The Lennard-Jones parameter ε_{LJ} is changed from[4] 2.1 kJ mol^{-1} to 1.6 kJ mol^{-1} in order to reduce the Lennard-Jones interaction between different CG methanol beads. The intrabead relative dielectric permittivity inside the cutoff sphere ε_{cs} is changed from[4] 2.5 to 1.6 to enhance the Coulomb interaction. The nonbonded interaction cutoff radius R_c is 2.0 nm. The properties of methanol measured experimentally and calculated from simulations using the FG and the two (old[4] and new) CG models of methanol are shown in Table 1.

2.2. Choice of the FG-CG Interaction for Methanol. As was observed for mixtures of CG and FG water,[38] when mixing CG and FG methanol, the distance between the positively charged DM site of a CG bead and the negatively charged oxygen (OMet) atom of FG methanol can become much smaller than between a DM site and the negatively charged CM site of another CG bead, thereby inducing a too strong DM-OMet electrostatic interaction. This is due to the rather different sizes of an FG molecule and a CG bead. To avoid too short distances between DM particles and FG atoms, we introduced a purely repulsive Lennard-Jones potential energy function for the interaction of DM sites with FG atoms of the solute as well as the FG solvent as in ref 38. The value of the Lennard-Jones C_{12} parameter for the interaction between DM sites and fine-grained OMet atoms was set to $7.7848\cdot10^{-9}$ kJ mol^{-1} nm^{12} which is 10 times the value used in mixtures of CG and FG water.[38] The value of C_{12} for the interaction between DM sites and FG CMet atoms is obtained using eq 1

$$C_{12}(DM - CMet) = \frac{\sqrt{C_{12}(CMet - CMet)}}{\sqrt{C_{12}(OMet - OMet)}} \cdot C_{12}(DM - OMet) \quad (1)$$

Since the hydrogen atom in the FG methanol model only interacts electrostatically, no C_{12}(DM-HMet) had to be defined. The value of C_{12} for the interaction between DM sites and FG atoms of the solute is obtained using eq 1 with the CMet atom type replaced by the various FG atom types of the solute. For the dielectric permittivity inside the cutoff sphere ε_{cs}^{mix} for the FG-CG interactions, the value 1.6 was found to adequately reproduce the free enthalpy of solvation of a single

FG methanol molecule and a single CG methanol bead (Table 2).

Table 2. Density ρ, Total Potential Energy Per Bead or Molecule for the CG-CG Interaction $V_{pot}^{CG\text{-}CG}$, the CG-FG Interaction $V_{pot}^{CG\text{-}FG}$, and the FG-FG Interaction $V_{pot}^{FG\text{-}FG}$, Surface Tension γ, Relative Static Dielectric Permittivity $\varepsilon(0)$, Free Enthalpy of Solvation ΔG_{solv} (FG;CG) of a Single FG Methanol Molecule in CG Methanol, and Free Enthalpy of Solvation ΔG_{solv} (CG;FG) of a Single CG Methanol Bead in FG Methanol for the 1:1 FG/CG Methanol Mixture at 298 K and 1 atm in Comparison with Experimental Data and Data from a Pure FG Methanol and from a Pure CG Methanol Simulation

	exp.[a]	pure FG	pure CG	FG/CG mixture
ρ [g/ cm^3]	0.787	0.786[b]	0.784	0.800
$V_{pot}^{CG\text{-}CG}$ [kJ/mol]			−16.9	−7.5
$V_{pot}^{CG\text{-}FG}$ [kJ/mol]				−9.1
$V_{pot}^{FG\text{-}FG}$ [kJ/mol]		−35.3		−27.5
γ [mN/m]	22.1	21.9[c]	18.0	16.2
$\varepsilon(0)$	32.6	19.8[b]	26.8	24.2
ΔG_{solv} (FG;FG) [kJ/mol]		−19.4		
ΔG_{solv} (FG;CG) [kJ/mol]			−19.7	
ΔG_{solv} (CG;CG) [kJ/mol]			−9.8	
ΔG_{solv} (CG;FG) [kJ/mol]		−11.2		

[a]From ref 64. [b]From ref 59. [c]From ref 4.

The C_{12} and C_6 Lennard-Jones parameters for the interaction between CM sites and FG particles are calculated using eqs 2 and 3

$$C_{12}(i,j) = 4\varepsilon_{ij}\sigma_{ij}^{12} \quad (2)$$

$$C_6(i,j) = 4\varepsilon_{ij}\sigma_{ij}^{6} \quad (3)$$

where ε_{ij} and σ_{ij} are calculated according to the combination rules used in GROMOS[48]

$$\sigma_{ij} = \sqrt{\sigma_i}\sqrt{\sigma_j} \quad (4)$$

$$\varepsilon_{ij} = \sqrt{\varepsilon_i}\sqrt{\varepsilon_j} \quad (5)$$

In contrast to the results from mixing CG and FG water,[38] the results for methanol to be discussed in the Results section showed that the C_{12} parameters for interactions between CM sites and FG particles calculated from the above equations had to be scaled by a factor of 1.3 in order to reproduce the properties of methanol in the mixture of FG/CG methanol.

2.3. Simulation of Mixtures of FG/CG Methanol. A 1:1 mixture of FG/CG methanol was used to find FG-CG interaction parameter sets that reproduce the thermodynamic and dielectric screening properties obtained from experiment or from MD simulations of pure FG or CG methanol. Since four FG methanol molecules are subsumed to one CG methanol bead, a cubic box of 3752 FG methanol molecules and 937 CG beads was used as the 1:1 FG/CG methanol mixture corresponded to a system of 7500 FG methanol molecules.

All simulations were carried out for 1 ns at a temperature of 298 K using the GROMOS[48−51] package of programs and the GROMOS force field 54A7.[6] The temperature was maintained using the weak coupling algorithm[52] with a coupling time of 0.1 ps, and the pressure was maintained close to 1 atm, except when calculating the surface tension γ, by weak coupling to a pressure bath with a coupling time of 0.5 ps and using an isothermal compressibility of $4.575\cdot10^{-4}$ (kJ mol^{-1} nm^{-3})$^{-1}$. For all simulations, nonbonded interactions were calculated using a triple-range scheme with a cutoff radii of 1.4/2.0 nm. Interactions within the short-range cutoff were evaluated every time step of 2 fs. The intermediate range interactions were updated every fifth time step, and the long-range electrostatic interactions were approximated by a reaction-field force[53] representing a continuum with a relative dielectric permittivity ε_{RF} of 32.63.[54] The geometry of the rigid FG methanol molecules was maintained using the procedure SHAKE[55] with a relative precision of 10^{-4}. The surface tension γ was calculated from a 1 ns NVT simulation, where the box length in the z-direction was extended to 40 nm which is five times longer than

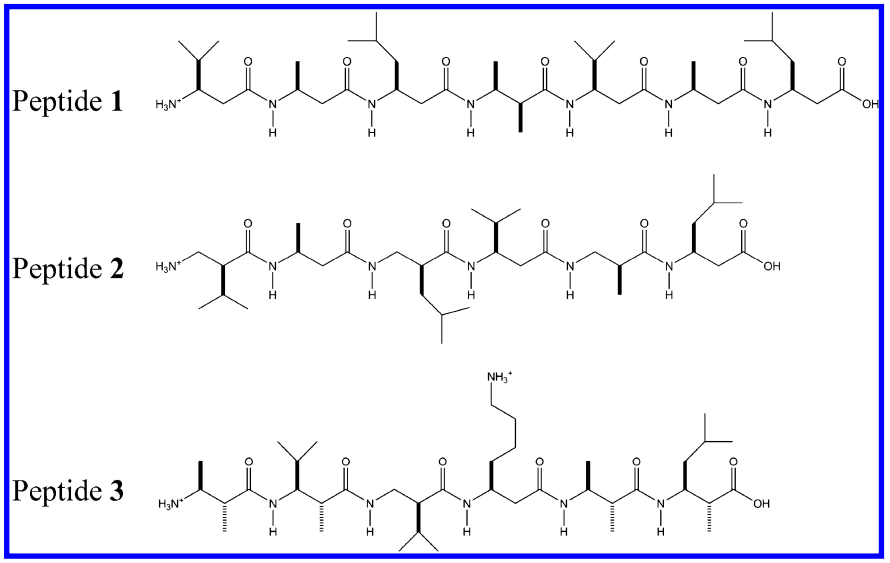

Figure 1. Chemical formulas of the three β-peptides: Peptide **1**, H_2^+-β^3-HVal-β^3-HAla-β^3-HLeu-(S,S)-β^3-HAla(αMe)-β^3-HVal-β^3-HAla-β^3-HLeu-OH; Peptide **2**, H_2^+-β^2-HVal-β^3-HAla-β^2-HLeu-β^3-HVal-β^2-HAla-β^3-HLeu-OH; Peptide **3**, H_2^+-(S,R)-β^3-HAla(αMe)-(S,R)-β^3-HVal(αMe)-β^2-HVal-β^3-HLys-(S,R)-β^3-HAla(αMe)-(S,R)-β^3-HLeu(αMe)-OH.

dx.doi.org/10.1021/ct500048c | J. Chem. Theory Comput. 2014, 10, 2213−2223

Table 3. Overview of the MD Simulations of the Peptides

peptide name	no. of residues	no. of peptide atoms	dominant fold	simulation name	no. of solvent molecules or beads	cutoff [nm]	efficiency[a] [ns/day]
peptide **1**	7	64	3_{14}-helix	1_{FG}	1096	0.8/1.4	25
				1_{CG}	365	1.4/2.0	114
				1_{FG_layer}	127/394[b]	1.4/2.0	63
peptide **2**	6	56	$2.7_{10/12}$-helix 3_{14}-helix	2_{FG}	1123	0.8/1.4	21
				2_{CG}	365	1.4/2.0	117
				2_{FG_layer}	120/467[b]	1.4/2.0	62
peptide **3**	6	64	hairpin	3_{FG}	1409	0.8/1.4	18
				3_{CG}	365	1.4/2.0	114
				3_{FG_layer}	144/455[b]	1.4/2.0	56

[a]Run on 8 CPUs using MPI parallelization. [b]FG/CG molecules.

the original length. The static dielectric permittivity $\varepsilon(0)$ was calculated using the external electric field method.[56] The external field strengths simulated ranged from 0.01 to 0.2 e·nm^{-2}, where the values from 0.01 to 0.1 e·nm^{-2} were considered for linear regression. Free enthalpies of solvation were calculated using thermodynamic integration (TI) of ensemble averages $\langle \partial H/\partial\lambda \rangle_\lambda$ in simulations using a coupling parameter λ dependent Hamiltonian H, with 21 equally spaced λ-values. A power of λ $n = 2$ was used.[57] The free enthalpies of solvation of a single FG methanol molecule in 1874 CG beads (ΔG_{solv}(FG;CG)) and of a single CG bead in 7496 FG methanol molecules (ΔG_{solv}(CG;FG)) were calculated in this manner.

In the same way, simulations of the 1:3 mixture consisting of 1875 FG methanol molecules and 1406 CG beads and the 3:1 mixture consisting of 5625 FG methanol molecules and 469 CG beads were carried out.

2.4. Simulation of Three β-Peptides Solvated in Methanol. Three β-peptides that adopt different dominant folds in methanol were used in this work, see Figure 1. Peptide **1** adopts predominantly a left-handed 3_{14} helical fold, peptide **2** adopts predominantly a right-handed $2.7_{10/12}$ helical fold, and peptide **3** adopts predominantly a hairpin fold, see Table 3.

Three different simulations, FG simulation, CG simulation, and FG_layer simulation, were carried out for 200 ns using the GROMOS[48−51] package of programs for all three β-peptides (see Table 3). The GROMOS force field[58] 54A7β was used. The experimentally determined dominant folded conformations of the three peptides were used as initial structures. For peptide **2**, the initial structure was the $2.7_{10/12}$-helix. In the FG simulations, each peptide was solvated in a periodic, rectangular box with methanol as solvent. The minimum distance from any peptide atom to the box wall was set to 1.4 nm in all cases. The resulting numbers of solvent molecules are listed in Table 3. In the CG simulations each peptide was solvated in a periodic, rectangular box with CG methanol beads as solvent. The sizes of the boxes were adjusted to contain 365 CG methanol beads. In the FG_layer simulations, each peptide was first solvated in FG methanol with a layer thickness of 0.8 nm, then the peptide together with the FG methanol layer was solvated in a periodic, rectangular box with CG methanol beads with the minimum distance from any FG methanol atom to the box wall of 1.0 nm. The resulting numbers of solvent molecules are also listed in Table 3. In order to keep the FG methanol molecules around the peptide in the FG_layer simulations, attractive harmonic distance restraints beyond a distance r_0 = 1.6 nm were applied between the oxygen atoms of the FG methanol molecules and the center of mass (COM) of the β-peptide approximated by the COM of four selected heavy atoms of the peptide, atoms C_α(3), N(4), O(4), and N(5) for peptide **1**, atoms C_α(3), C(3), N(4), and C_β(4) for peptide **2**, and atoms C_β(2), C(2), N(5), and C_α(5) for peptide **3**. The force constant is 300 kJ mol^{-1} nm^{-2}. The details of the technique to keep a layer of FG solvent around a solute is described in ref 40. Figure 2 shows

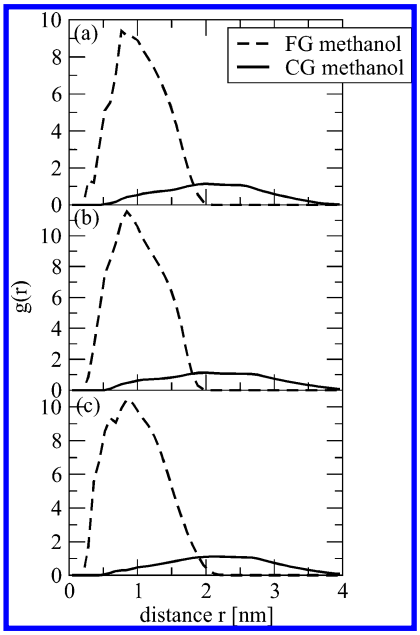

Figure 2. Radial distribution function $g(r)$ of FG methanol (dashed) and CG methanol (solid), where r represents the distance between the OMet atoms of FG methanol or CM paticles of CG methanol and the center of geometry of the peptides. (a) 1_{FG_layer}, (b) 2_{FG_layer}, (c) 3_{FG_layer}. The simulation names are specified in Table 3.

that the FG methanol molecules are kept near the solute. The restraining energies are with average values of 22 to 24 kJ mol^{-1} only a small fraction of the average potential energy (−10^4 kJ mol^{-1}), see Table 4.

All simulations were carried out at the temperature 340 K and a constant pressure of 1 atm using the weak coupling algorithm.[52] The temperature coupling time was set to 0.1 ps, the pressure coupling time was set to 0.5 ps, and isothermal compressibility was set to $4.575 \cdot 10^{-4}$ (kJ mol^{-1} nm^{-3})$^{-1}$. For all simulations, nonbonded interactions were calculated using a triple-range scheme with cutoff radii of 1.4/2.0 nm for mixed-grained simulations and 0.8/1.4 nm for FG simulations. Interactions within the short-range cutoff were evaluated every time step. The intermediate range interactions were

Table 4. Potential Energies in Simulation 1_{FG_layer}, 2_{FG_layer}, and 3_{FG_layer}[a]

potential energy [kJ mol^{-1}]	1_{FG_layer}	2_{FG_layer}	3_{FG_layer}
U_{pot}	−10352	−10851	−11734
U_{bonded}	543	628	608
$U_{LJ}^{peptide-peptide}$	−109	−84	−82
$U_{LJ}^{peptide-FGsv}$	−113	−108	−132
$U_{LJ}^{peptide-CGsv}$	−48	−45	−39
$U_{CRF}^{peptide-peptide}$	−778	−659	−615
$U_{CRF}^{peptide-FGsv}$	−450	−477	−1031
$U_{CRF}^{peptide-CGsv}$	−2	−8	−23
U_{disres}	23	22	24

[a] U_{pot} is the total potential energy. U_{bonded} is the bonded potential energy. $U_{LJ}^{peptide-peptide}$ is the intrapeptide Lennard-Jones potential energy. $U_{LJ}^{peptide-FGsv}$ is the Lennard-Jones potential energy between peptide and FG solvent. $U_{LJ}^{peptide-CGsv}$ is the Lennard-Jones potential energy between peptide and CG solvent. $U_{CRF}^{peptide-peptide}$ is the intrapeptide Coulomb plus reaction field potential energy. $U_{CRF}^{peptide-FGsv}$ is the Coulomb plus reaction field potential energy between peptide and FG solvent. $U_{CRF}^{peptide-CGsv}$ is the Coulomb plus reaction field potential energy between peptide and CG solvent. U_{disres} is total distance restraining energy.

updated every fifth time step of 2 fs, and the long-range electrostatic interactions were approximated by a reaction-field force[53] representing a continuum with a relative dielectric permittivity ε_{RF} of[54] 32.63 in mixed-grained simulations and of[59] 19.8 in FG simulations. The bond lengths of the solute were kept rigid using the procedure SHAKE[55] with a precision of 10^{-4}.

The three peptides were also simulated in vacuo using the GROMOS force field[6] 54A7, using the vacuum GROMOS force field[6] 54B7 and using the latter plus an additional solvent-accessible-surface-area (SASA) potential energy term[60] mimicking implicit solvation forces. In the 54B7 vacuum force field moieties bearing a full charge (Lys, N-terminus) are made neutral without loss of their hydrogen-bonding capabilities by a reduction of partial charges and the repulsive Lennard-Jones parameters.[48,61] The SASA term is specified and validated in ref 60. The computational setup of these vacuum simulations is as specified in ref 39 for four proteins. The results are given in the Supporting Information.

2.5. Analysis. *2.5.1. Mixtures of FG/CG Methanol.* The density of the mixture and potential energies between CG-CG, CG-FG, and FG-FG particles were calculated using the GROMOS analysis program *ene_ana*.[49] The surface tension γ, relative static dielectric permittivity $\varepsilon(0)$, self-diffusion coefficient D, local compositions of CG beads and of FG methanol molecules, and free enthalpy of solvation were calculated as described in ref 38. The thermal expansion coefficient α_p, heat capacity C_p, and isothermal compressibility κ_T were calculated in the same way as described in ref 4.

The change of enthalpy upon mixing ΔH_{mix} was calculated as

$$\Delta H_{mix} = U(mix) - x_{FG}U(FG) - (1 - x_{FG})U(CG) \quad (6)$$

where $U(mix)$ is the potential energy of the mixture, and $U(FG)$ and $U(CG)$ are the potential energies of the pure FG and CG simulations.

The change of volume upon mixing ΔV_{mix} was calculated as

$$\Delta V_{mix} = V(mix) - x_{FG}V(FG) - (1 - x_{FG})V(CG) \quad (7)$$

where $V(mix)$ is the volume of the mixture, and $V(FG)$ and $V(CG)$ are the volumes of the pure FG and CG simulations.

2.5.2. β-Peptide Folding in FG and CG Methanol. Trajectory coordinates and energies stored at 0.5 ps intervals were used for analysis. Backbone atom-positional root-mean-square differences (RMSD) between two solute conformations were calculated after translational superposition of the solute centers of mass and least-squares rotational fitting of atomic positions, using all backbone atoms (N,CB,CA,C) of residues 2−6 for peptide **1** and of residues 2−5 for peptide **2** and peptide **3**. Hydrogen bonds were defined by a maximum hydrogen-acceptor distance of 0.25 nm and a minimum donor-hydrogen-acceptor angle of 135°. Hydrogen-hydrogen distances extracted from the NOE intensities measured in the NMR experiments were compared with the corresponding average distances in the simulations calculated using $\langle r^{-6}\rangle^{-1/6}$, i.e. r^{-6} averaging, where r is the instantaneous hydrogen-hydrogen distance. Hydrogen-hydrogen distances involving aliphatic hydrogen atoms were calculated by defining virtual (CH_1), prochiral (stereospecific CH_2), and pseudo (CH_3 and nonstereospecific CH_2) atomic positions, and pseudoatom corrections were added to the distance bounds for the latter, 0.1 nm for nonstereospecific CH_2, 0.15 nm for CH_3, and 0.29 nm for nonstereospecific rotating methyls.[62] We do not calculate ^{3}J-couplings for the peptides, because the Karplus relation between torsional angle and corresponding ^{3}J-coupling is with an imprecision of at least 2 Hz rather approximate.[63]

For the FG_layer simulations, the radial distribution function (RDF) $g(r)$ of the CM sites of the CG beads and the oxygen atoms of the FG methanol molecules around the center of geometry (COG) of the peptides was calculated as

$$g(r) = \frac{N_J(k)}{4\pi r^2 dr \rho_J} \quad (8)$$

where $N_J(k)$ is the number of CM sites or oxygen atoms found at a distance $r(k)-1/2dr$ and $r(k)+1/2dr$, the discrete distances $r(k)$ are separated by a distance dr, and ρ_J is the number density of particles J.

3. RESULTS

3.1. Mixtures of FG/CG Methanol. The properties of the 1:1 FG/CG methanol mixture simulated with the FG/CG interaction parameter set and the corresponding experimental data and the averages for the pure FG or CG methanol system are shown in Table 2. A dielectric permittivity $\varepsilon_{cs}^{mix} = 1.6$ inside the cutoff sphere for the FG-CG interactions was used. With the scaling factor 1.3 of the C_{12} Lennard-Jones parameter between CM sites and FG particles, the density of the mixture is 0.800 g·cm^{-3} which is only 1.7% larger than the experimental value[64] of 0.787 g·cm^{-3}. The potential energy per bead or molecule of the mixture is comparable to the reference data from the pure FG or CG simulation, if we add up V_{pot}^{CG-CG} and V_{pot}^{CG-FG} or V_{pot}^{FG-FG} and V_{pot}^{CG-FG}, respectively. The surface tension γ and relative static dielectric permittivity $\varepsilon(0)$ of the mixture are also close to the data calculated from the pure CG simulation. The free enthalpy of solvation ΔG_{solv}(FG;CG) of a single FG methanol molecule in CG methanol is very close to the reference value ΔG_{solv}(FG;FG), and ΔG_{solv}(CG;FG) of a single CG bead in FG methanol is a bit more negative than the reference value ΔG_{solv}(CG;CG). The FG/CG interaction parameter set was used for the subsequent simulations of 1:3 and 3:1 FG/CG methanol mixtures and the simulations of β-peptide folding in pure CG methanol or with an FG methanol layer.

dx.doi.org/10.1021/ct500048c | J. Chem. Theory Comput. 2014, 10, 2213−2223

The local compositions of the FG methanol molecules $x_{OMet\text{-}OMet}(r)$ and of the CG beads $x_{CM\text{-}CM}(r)$ in FG/CG methanol mixtures are shown in Figure 3. The local composition measures the amount of neighbors as a function of the distance. For very short distances, the FG molecules are surrounded only by other FG molecules in all mixtures, i.e., $x_{OMet\text{-}OMet}(r) = 1$, as the CG beads cannot come close due to their size. Then there is drop in $x_{OMet\text{-}OMet}(r)$ caused by the presence of CG beads. The CG beads on the other hand are surrounded at most by 50% CG beads at $r \approx 0.65$ nm in the 1:3 FG/CG mixtures, which corresponds to the CM-CM distance in pure CG methanol.

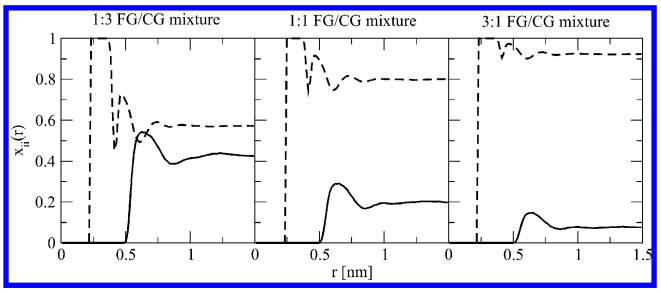

Figure 3. Local compositions $x_{CM\text{-}CM}(r)$ of CG beads (solid) and $x_{OMet\text{-}OMet}(r)$ of FG methanol molecules (dashed) in 1:3, 1:1, and 3:1 (v%/v%)FG/CG mixtures at 298 K and 1 atm.

The other properties of the FG/CG methanol mixtures are shown in Figure 4. As mentioned before, ΔG_{solv}(CG;FG) of a single CG bead in FG methanol is a bit more negative than the value ΔG_{solv}(CG;CG), the interaction between CG and FG methanol is a bit stronger than that between CG-CG beads, so the density of the mixtures is higher than that of pure FG or CG methanol, especially in the 1:1 mixture. Correspondingly, the change of volume upon mixing, ΔV_{mix}, is negative.

3.2. β-Peptide Folding in Explicit FG and CG Methanol. *3.2.1. Peptide 1.* The atom-positional RMSD of the backbone atoms of residues 2 to 6 with respect to the 3_{14}-helical model structure are shown in Figure 5 for MD simulations of peptide **1** at 340 K and 1 atm as a function of the simulation time together with their distributions. The helical fold of the peptide is stable in all three simulations. In simulation 1_{CG} the peptide is most stable compared to the other simulations. The RMSD distribution of simulation 1_{FG_layer} is similar to that of simulation 1_{FG}.

Populations of intramolecular 3_{14}-helical hydrogen bonds, i.e. those between NH(i) and O(i+2) with residue sequence number i, in the simulations of peptide **1** are listed in Table 5. The populations of intramolecular 3_{14}-helical hydrogen bonds are higher in simulation 1 CG than those in simulation 1_{FG}, especially at the two ends of the peptide. This is due to the lack of hydrogen-bonding partners in the CG solvent. The populations of intramolecular 3_{14}-helical hydrogen bonds in simulation 1_{FG_layer} are also higher than those in simulation 1_{FG}, but the populations of intramolecular hydrogen bonds at the

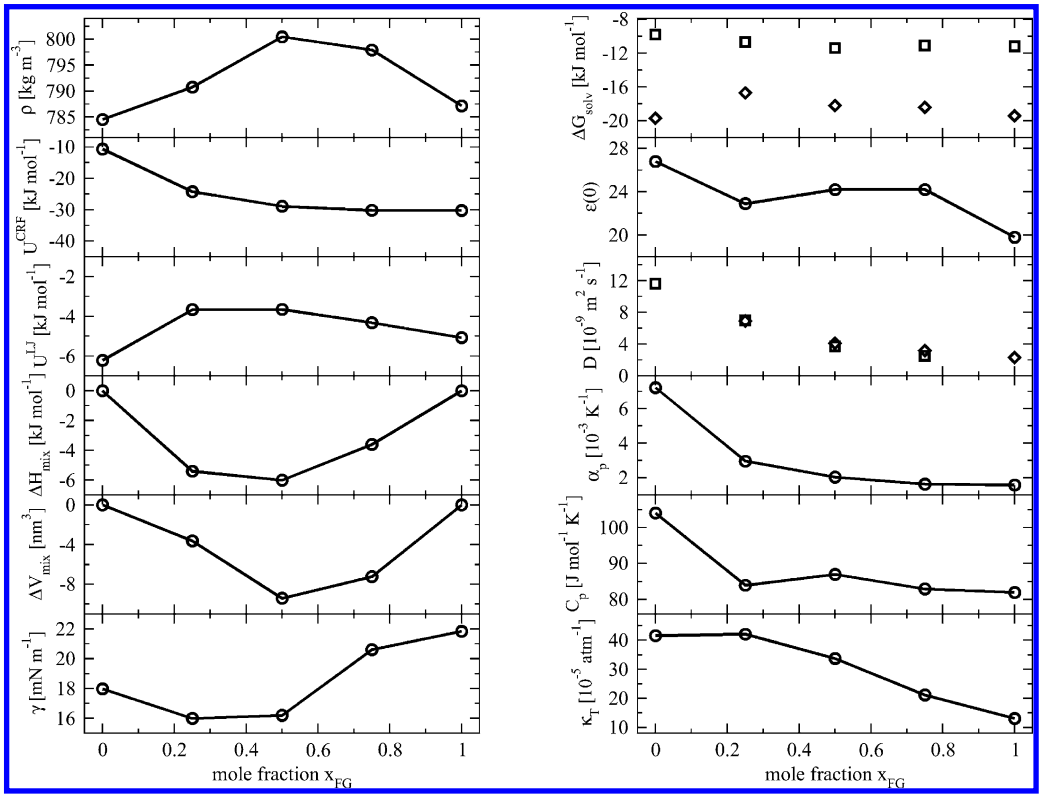

Figure 4. Properties for the mixtures of FG and CG methanol. x_{FG} is the mole fraction of FG methanol molecules. ρ = density. U^{CRF} = Coulomb plus reaction field potential energy per bead or molecule. U^{LJ} = Lennard-Jones potential energy per bead or molecule. ΔH_{mix} = change of enthalpy upon mixing. ΔV_{mix} = change of volume upon mixing. γ = surface tension. ΔG_{solv} = free enthalpy of solvation of a single FG methanol molecule (diamond) and a single CG methanol bead (square) in the mixtures. $\varepsilon(0)$ = dielectric permittivity. D = diffusion constant of FG methanol molecules (diamond) and CG methanol beads (square). C_p = heat capacity per bead or molecule at constant pressure. α_p = thermal expansion coefficient. κ_T = isothermal compressibility.

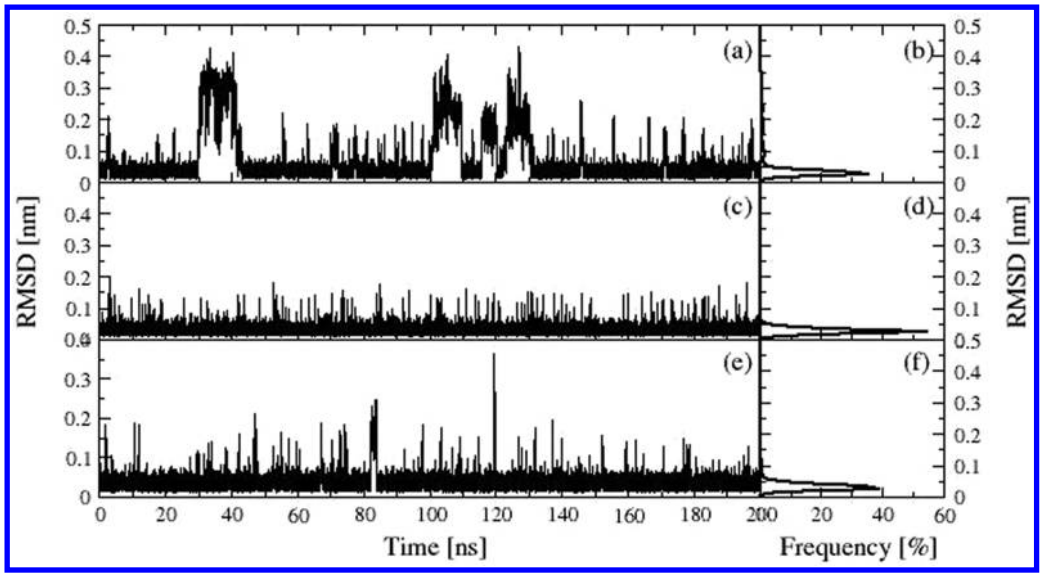

Figure 5. Time evolution (left panels) and distribution (right panels) of the atom-positional RMSD from the 3_{14}-helical model structure for the backbone atoms of residues 2−6 in 200 ns MD simulations of peptide **1** at 340 K. (a, b) 1_{FG}; (c, d) 1_{CG}; (e, f) 1_{FG_layer}. The simulation names are specified in Table 3.

Table 5. Intramolecular Hydrogen-Bond Populations (in %) of Three β-Peptides in 200 ns MD Simulations at 340 K and 1 atm Using the GROMOS 54A7β Force Field and Using an FG Methanol Solvent, a CG Methanol Solvent, and the Latter with an FG Methanol Layer around the Peptide

donor···acceptor	FG	CG	FG_layer
Peptide **1**			
[H-bonds of 3_{14}-helix]			
NH(1)···O(3)	22	85	33
NH(2)···O(4)	76	88	93
NH(3)···O(5)	81	90	95
NH(4)···O(6)	78	97	93
NH(5)···O(7)	32	81	47
Peptide **2**			
[H-bonds of $2.7_{10/12}$-helix]			
NH(3)···O(4)	46	1	30
NH(4)···O(1)	19	0.5	21
NH(6)···O(3)	42	3	32
[H-bonds of 3_{14}-helix]			
NH(1)···O(3)	7	85	27
NH(2)···O(4)	15	88	48
NH(3)···O(5)	13	87	44
NH(4)···O(6)	12	86	42
Peptide **3**			
[H-bonds of hairpin]			
NH(1)···O(6)	1	17	1
NH(2)···O(5)	5	0	3
NH(3)···O(4)	51	0	29

two ends of the peptide are much lower than those in simulation 1_{CG}. It shows that the introduction of an FG methanol layer around the peptide may recover the hydrogen-bonding pattern of the FG simulation.

The hydrogen-hydrogen NOE distance bound violations calculated from the simulations of peptide **1** are shown in Figure 6. Thirty-three NOEs are between hydrogens within a residue or in residues adjacent in the amino-acid sequence.[45] NOEs 7, 16, and 24 are between residues *i* and *i*+2, while NOEs 8, 17, 25, 26, 32, and 38 are between residues *i* and *i*+3.

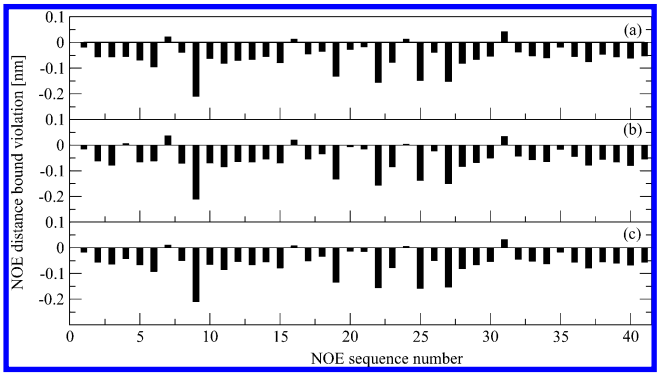

Figure 6. Difference of $\langle r^{-6}\rangle^{-1/6}$ as obtained from 200 ns MD simulations at 340 K and 1 atm and NOE atom-atom distance (r) bounds as derived from experimental NMR data[67] at 298 K for 41 atom-atom pairs in peptide **1**. (a) 1_{FG}; (b) 1_{CG}; (c) 1_{FG_layer}. The simulation names are specified in Table 3. The list of NOEs is specified in ref 45.

Four slightly positive violations, No. 7, $H_N(2)$-$H_\beta(4)$, No. 16, $H_N(3)$-$H_\beta(5)$, No. 24, $H_N(4)$-$H_\beta(6)$, and No. 31, $H_N(5)$-$H_N(6)$, appeared in all three simulations; they are lowest in simulation 1_{FG_layer}. Interestingly, although the peptide is most stable in simulation 1_{CG}, there is one more slightly positive violation (No. 4, $H_N(2)$-$H_\alpha(4)$) in this simulation. However, all these positive violations are rather insignificant considering the accuracy of the NMR derived NOE distance bounds.

3.2.2. Peptide 2. The conformational ensemble of peptide **2** contains both right-handed $2.7_{10/12}$-helical and left-handed 3_{14}-helical conformations.[65] Reproduction of this conformational equilibrium is therefore a sensitive force-field test. The atom-positional RMSD of the backbone atoms of residues 2 to 5 of peptide **2** with respect to a $2.7_{10/12}$-helical structure or to a 3_{14}-helical structure are shown in Figure 7. The FG simulation samples both dominant helical folds. In simulation 2_{CG} starting from a right-handed $2.7_{10/12}$-helical structure the peptide converts to a left-handed 3_{14}-helical conformation which is maintained during 190 ns. When introducing an FG methanol layer, both helical conformations are sampled in simulation

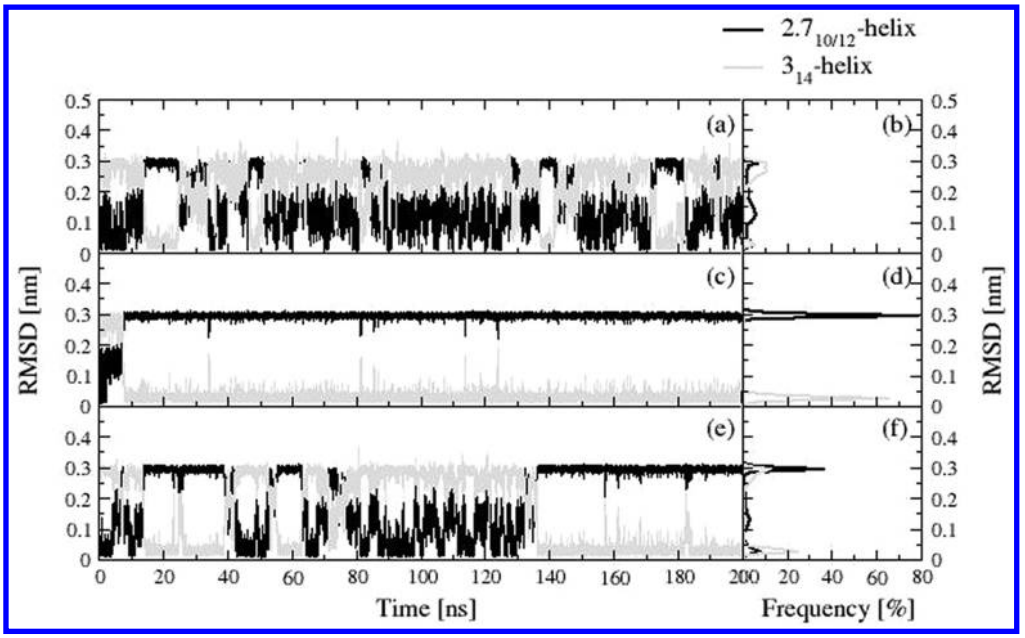

Figure 7. Time evolution (left panels) and distribution (right panels) of atom-positional RMSD with respect to a right-handed $2.7_{10/12}$-helix (black lines) and with respect to a left-handed 3_{14}-helix (gray lines) for the backbone atoms of residues 2−5 in 200 ns MD simulations of peptide **2** at 340 K. (a, b) 2_{FG}; (c, d) 2_{CG}; (e, f) 2_{FG_layer}. The simulation names are specified in Table 3.

2_{FG_layer}. Populations of intramolecular $2.7_{10/12}$- and 3_{14}-helical hydrogen bonds in the simulations of peptide **2** at 340 K are listed in Table 5. The dominance of the 3_{14}-helical conformation in simulation 2 CG could be due to the presence of one more intramolecular hydrogen bond in a 3_{14}-helix than in a $2.7_{10/12}$-helix. The former helix would be more favored in pure CG solvent which lacks hydrogen-bonding partners for the solute.

The hydrogen-hydrogen NOE distance bound violations calculated from the simulations of peptide **2** are shown in Figure 8. Twenty-two NOEs are between hydrogens within a residue or in residues adjacent in the amino-acid sequence.[45] NOEs 2, 10, 15, 16, 19, 26, 27, and 28 are between residues *i* and *i*+2, while NOEs 3 and 18 are between residues *i* and *i*+3.

Simulation 2_{FG} shows slight violations for six NOEs, No. 3, $H_\alpha(1)$-$H_\beta(4)$, No. 10, $H_\beta(2)$-$H_\alpha(4)$, No. 16, $H_\beta(3)$-$H_\alpha(1)$, No. 19, $H_N(4)$-$H_\beta(2)$, No. 27, $H_N(6)$-$H_\beta(4)$, and No. 28, $H_N(6)$-$H_\alpha^{Si}(4)$. Simulation 2_{CG} shows six rather large violations and three slight violations. Because only 3_{14}-helical conformations are sampled, the NOE bounds characteristic for a $2.7_{10/12}$-helix are violated. Similar to simulation 2_{FG}, simulation 2_{FG_layer} also shows only small NOE bound violations, indicating that both R- and L-helical structures are sampled.

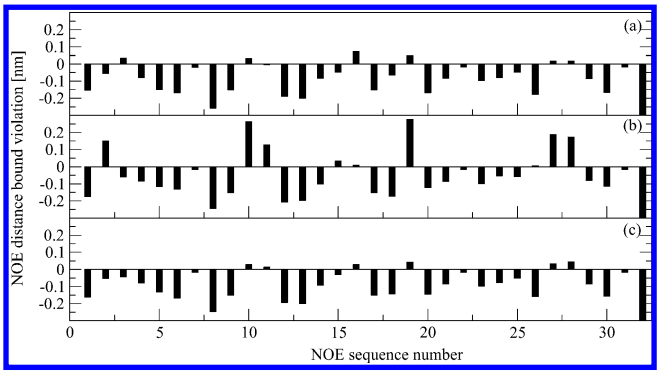

Figure 8. Difference of $<r^{-6}>^{-1/6}$ as obtained from 200 ns MD simulations at 340 K and 1 atm and NOE atom-atom distance (r) bounds as derived from experimental NMR data[68] at 298 K for 32 atom-atom pairs in peptide **2**. (a) 2_{FG}; (b) 2_{CG}; (c) 2_{FG_layer}. The simulation names are specified in Table 3. The list of NOEs is specified in ref 45.

*3.2.3. Peptide **3**.* The atom-positional RMSD of the backbone atoms of residues 2 to 5 with respect to the model hairpin structure (X-PLOR structure number 1[44]) are shown in Figure 9 for simulations of peptide **3** at 340 K and 1 atm as a function of the simulation time together with their distributions. The RMSD distributions of simulation 3_{FG} and 3_{FG_layer} are similar. In contrast, the hairpin structure is rarely sampled in simulation 3_{CG}. The populations of intramolecular hairpin hydrogen bonds yield the same picture (see Table 5).

The hydrogen-hydrogen NOE distance bound violations calculated from the simulations of peptide **3** are shown in Figure 10. Seventeen NOEs are between hydrogens within a residue or in residues adjacent in the amino-acid sequence.[45] NOEs 19 and 20 are between residues *i* and *i*+3, while NOE 18 is between residues *i* and *i*+5. There are two positive violations in all three simulations, No. 18, $H_\alpha(1)$-$H_\beta(6)$ and No. 19, $H_\alpha(2)$-$H_\beta(5)$, corresponding to a hairpin structure. They are quite large in simulation 3_{CG}, because the hairpin conformations are not sampled in this simulation. They are rather small in simulation 3_{FG} and 3_{FG_layer}.

3.2.4. Computational Efficiency. The computational efficiency of each β-peptide simulation is listed in Table 3. All simulations were run on 8 CPUs using MPI parallelization. In the mix-grained simulations (CG simulation and FG_layer simulation), the solvent beads represent four FG methanol molecules. The CG simulation is 5−6 times faster than the FG simulation, and the FG_layer simulation is 3 times faster than the FG simulation, although a much larger cutoff for the nonbonded interactions is used in the mixed-grained simulations, i.e. 1.4/2.0 nm versus 0.8/1.4 nm in the FG simulations. If the same cutoff radii had been used in FG and

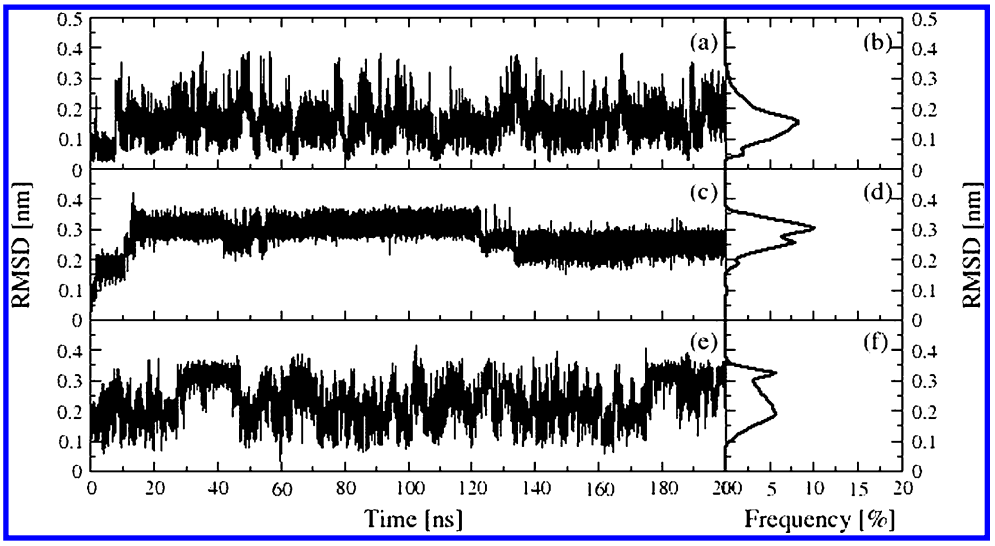

Figure 9. Time evolution (left panels) and distribution (right panels) of the atom-positional RMSD from the model hairpin structure for the backbone atoms of residues 2−5 in 200 ns MD simulations of peptide **3** at 340 K. (a, b) 3_{FG}; (c, d) 3_{CG}; (e, f) 3_{FG_layer}. The simulation names are specified in Table 3.

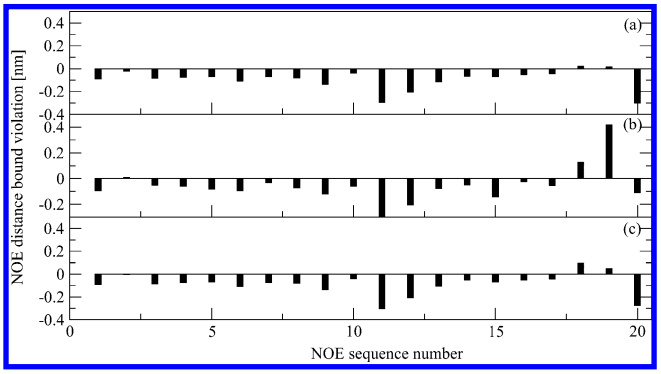

Figure 10. Difference of $\langle r^{-6}\rangle^{-1/6}$ as obtained from 200 ns MD simulations at 340 K and 1 atm and NOE atom-atom distance (r) bounds as derived from experimental NMR data[44] at 298 K for 20 atom-atom pairs in peptide **3**. (a) 3_{FG}; (b) 3_{CG}; (c) 3_{FG_layer}. The simulation names are specified in Table 3. The list of NOEs is specified in ref 45.

mix-grained simulations, the latter would have been more than an order of magnitude faster.

3.2.5. β-Peptide Folding in Vacuo or Using Implicit Solvation. One may ask whether it would be possible to simulate the β-peptide folding equilibria using even more approximate solvent models than the FG and CG methanol models applied so far. In Figures S1-S6 of the Supporting Information the RMSD values and NOE distance bound violations in simulations using the 54A7 force field for condensed-phase simulations without any solvent molecules, using the 54B7 force field for vacuum simulations, and using the latter with an additional solvent-accessible-surface-area (SASA) term as an implicit solvation representation are shown. These figures correspond to Figures 5-10 showing the explicit solvation results. Table S1 contains the implicit solvation hydrogen-bond occurrences corresponding to the explicit solvation ones in Table 5.

The 3_{14}-helical fold of peptide **1** shows less helical hydrogen bonding in implicit solvent or vacuum, and only the SASA implicit solvation term induces refolding after unfolding (Table S4, Figure S1). The NOE distance bound violations are larger than in explicit solvent (Figure S2). They are still not, apart from the 54B7 simulation, very large, because the dominant 3_{14}-helical structure was used as starting structure.

The equilibrium between the R- and L-helical folds of peptide **2** is only partially obtained using the 54B7 force field (Table S1, Figure S3), but no complete transitions from the $2.7_{10/12}$-helix to the 3_{14}-helix are occurring. This picture is confirmed by the pattern of NOE distance bound violations (Figure S4) showing the lowest violations for force field 54B7.

The hairpin structure of peptide **3** is only partly maintained using the 54A7 force field, probably due to the full charges stabilizing the hairpin starting structure (Table S1, Figure S5). This makes this simulation still satisfy the NOE distance bounds due to the r^{-6} averaging.

In summary, none of the implicit or vacuum simulations satisfy the experimental NMR data as well as the explicit solvation ones.

4. CONCLUSION

Combination of an atomic-level, fine-grained (FG) model for a peptidic solute with a supramolecular, coarse-grained (CG) model for the solvent allows an efficient sampling of the folding equilibria of polypeptides. In the present study, the folding equilibria of three β-peptides that fold into different folds in methanol were investigated using such hybrid FG/CG simulations. First, the CG methanol model of ref 4 was reparametrized because its ratio of Lennard-Jones and electrostatic interactions was 2:1 instead of 1:2 as in the FG methanol model to be used in conjunction with the CG methanol model. A prerequisite for the latter is a proper calibration of the FG-CG interactions using thermodynamic data for the solvent. Using a 1:1 mixture of FG and CG methanol, a FG-CG interaction parameter set was determined which was subsequently tested in mixed-grained simulations of three β-peptides. The properties of the β-peptides were compared to those obtained from FG simulations and from experimental NMR data.

The comparison of the backbone atom-positional RMSD with respect to the dominant folds of the peptides, of intramolecular hydrogen bonds, and of NOE distance upper

bound violations shows that the conformational ensembles of the peptides in the pure CG solvent simulations are different from those of the FG simulations because of the lack of hydrogen-bonding partners in the CG solvent. The introduction of an FG solvent layer in the mixed-grained simulations can solve this problem. The conformational ensembles and structural properties of the FG_layer simulations are similar to those of the FG solvent simulations. Although the introduction of an FG solvent layer will halve the computational efficiency compared with the pure CG solvent simulation, it is still at least 3 times faster than the FG solvent simulation.

The comparisons of the simulations using the CG solvent with those using a vacuum boundary condition or a vacuum adapted force field or the latter plus an implicit solvation term show that the latter display larger differences with respect to experimental NMR data and when compared to the use of an FG molecular solvent than observed when using a CG supramolecular solvent with an FG solvent layer.

■ ASSOCIATED CONTENT

Supporting Information

The three peptides were also simulated in vacuo using the GROMOS force field[6] 54A7, using GROMOS vacuum force field[6] 54B7, and using the latter plus an additional solvent-accessible-surface-area (SASA) potential energy term[60] mimicking implicit solvation forces. Intrasolute hydrogen-bond occurrences for the three peptides are given in Table S1. Time evolutions and distributions of the atom-positional RMSD from helical or hairpin structures for the three peptides are given in Figures S1, S3, and S5. The NOE distance-bound violations are given in Figures S2, S4, and S6. This material is available free of charge via the Internet at http://pubs.acs.org.

■ AUTHOR INFORMATION

Corresponding Author

*E-mail: wfvgn@igc.phys.chem.ethz.ch.

Notes

The authors declare no competing financial interest.

■ ACKNOWLEDGMENTS

This work was financially supported by the National Center of Competence in Research (NCCR) in Structural Biology, by grant number 200020-137827 of the Swiss National Science Foundation, and by grant number 228076 of the European Research Council (ERC), which is gratefully acknowledged.

■ REFERENCES

(1) Shaw, D. E.; Deneroff, M. M.; Dror, R. O.; Kuskin, J. S.; Larson, R. H.; Salmon, J. K.; Young, C.; Batson, B.; Bowers, K. J.; Chao, J. C.; Eastwood, M. P.; Gagliardo, J.; Grossman, J. P.; Ho, C. R.; Ierardi, D. J.; Kolossvary, I.; Klepeis, J. L.; Layman, T.; Mcleavey, C.; Moraes, M. A.; Mueller, R.; Priest, E. C.; Shan, Y. B.; Spengler, J.; Theobald, M.; Towles, B.; Wang, S. C. *Commun. ACM* **2008**, *51*, 91−97.

(2) Riniker, S.; Allison, J. R.; van Gunsteren, W. F. *Phys. Chem. Chem. Phys.* **2012**, *14*, 12423−12430.

(3) Riniker, S.; van Gunsteren, W. F. *J. Chem. Phys.* **2011**, *134*, 084110.

(4) Allison, J. R.; Riniker, S.; van Gunsteren, W. F. *J. Chem. Phys.* **2012**, *136*, 054505.

(5) Schuler, L. D.; Daura, X.; van Gunsteren, W. F. *J. Comput. Chem.* **2001**, *22*, 1205−1218.

(6) Schmid, N.; Eichenberger, A. P.; Choutko, A.; Riniker, S.; Winger, M.; Mark, A. E.; van Gunsteren, W. F. *Eur. Biophys. J.* **2011**, *40*, 843−856.

(7) Tschop, W.; Kremer, K.; Hahn, O.; Batoulis, J.; Burger, T. *Acta Polym.* **1998**, *49*, 75−79.

(8) Izvekov, S.; Voth, G. A. *J. Phys. Chem. B* **2005**, *109*, 2469−2473.

(9) Milano, G.; Müller-Plathe, F. *J. Phys. Chem. B* **2005**, *109*, 18609−18619.

(10) Izvekov, S.; Voth, G. A. *J. Chem. Phys.* **2005**, *123*, 134105.

(11) Praprotnik, M.; Delle Site, L.; Kremer, K. *J. Chem. Phys.* **2005**, *123*, 224106.

(12) Neri, M.; Anselmi, C.; Cascella, M.; Maritan, A.; Carloni, P. *Phys. Rev. Lett.* **2005**, *95*, 218102.

(13) Harmandaris, V. A.; Adhikari, N. P.; van der Vegt, N. F. A.; Kremer, K. *Macromolecules* **2006**, *39*, 6708−6719.

(14) Praprotnik, M.; Delle Site, L.; Kremer, K. *Phys. Rev. E* **2006**, *73*, 066701.

(15) Christen, M.; van Gunsteren, W. F. *J. Chem. Phys.* **2006**, *124*, 154106.

(16) Lyman, E.; Ytreberg, F. M.; Zuckerman, D. M. *Phys. Rev. Lett.* **2006**, *96*, 028105.

(17) Shi, Q.; Izvekov, S.; Voth, G. A. *J. Phys. Chem. B* **2006**, *110*, 15045−15048.

(18) Shih, A. Y.; Freddolino, P. L.; Sligar, S. G.; Schulten, K. *Nano Lett.* **2007**, *7*, 1692−1696.

(19) Heath, A. P.; Kavraki, L. E.; Clementi, C. *Proteins: Struct., Funct., Bioinf.* **2007**, *68*, 646−661.

(20) Praprotnik, M.; Matysiak, S.; Delle Site, L.; Kremer, K.; Clementi, C. *J. Phys.: Condens. Matter* **2007**, *19*, 292201.

(21) Ensing, B.; Nielsen, S. O.; Moore, P. B.; Klein, M. L.; Parrinello, M. *J. Chem. Theory Comput.* **2007**, *3*, 1100−1105.

(22) Liu, P.; Voth, G. A. *J. Chem. Phys.* **2007**, *126*, 045106.

(23) Carpenter, T.; Bond, P. J.; Khalid, S.; Sansom, M. S. P. *Biophys. J.* **2008**, *95*, 3790−3801.

(24) Heyden, A.; Truhlar, D. G. *J. Chem. Theory Comput.* **2008**, *4*, 217−221.

(25) Matysiak, S.; Clementi, C.; Praprotnik, M.; Kremer, K.; Delle Site, L. *J. Chem. Phys.* **2008**, 128.

(26) Praprotnik, M.; Delle Site, L.; Kremer, K. *Annu. Rev. Phys. Chem.* **2008**, *59*, 545−571.

(27) Michel, J.; Orsi, M.; Essex, J. W. *J. Phys. Chem. B* **2008**, *112*, 657−660.

(28) Masella, M.; Borgis, D.; Cuniasse, P. *J. Comput. Chem.* **2008**, *29*, 1707−1724.

(29) Park, J. H.; Heyden, A. *Mol. Simul.* **2009**, *35*, 962−973.

(30) Rzepiela, A. J.; Schafer, L. V.; Goga, N.; Risselada, H. J.; De Vries, A. H.; Marrink, S. J. *J. Comput. Chem.* **2010**, *31*, 1333−1343.

(31) Poblete, S.; Praprotnik, M.; Kremer, K.; Delle Site, L. *J. Chem. Phys.* **2010**, *132*, 114101.

(32) Samiotakis, A.; Homouz, D.; Cheung, M. S. *J. Chem. Phys.* **2010**, *132*, 175101.

(33) Izvekov, S.; Chung, P. W.; Rice, B. M. *J. Chem. Phys.* **2010**, *133*, 064109.

(34) Junghans, C.; Poblete, S. *Comput. Phys. Commun.* **2010**, *181*, 1447−1452.

(35) Masella, M.; Borgis, D.; Cuniasse, P. *J. Comput. Chem.* **2011**, *32*, 2664−2678.

(36) Rzepiela, A. J.; Louhivuori, M.; Peter, C.; Marrink, S. J. *Phys. Chem. Chem. Phys.* **2011**, *13*, 10437−10448.

(37) Bezkorovaynaya, O.; Lukyanov, A.; Kremer, K.; Peter, C. *J. Comput. Chem.* **2012**, *33*, 937−949.

(38) Riniker, S.; van Gunsteren, W. F. *J. Chem. Phys.* **2012**, *137*, 044120.

(39) Riniker, S.; Eichenberger, A. P.; van Gunsteren, W. F. *Eur. Biophys. J.* **2012**, *41*, 647−661.

(40) Riniker, S.; Eichenberger, A. P.; van Gunsteren, W. F. *J. Phys. Chem. B* **2012**, *116*, 8873−8879.

(41) van Gunsteren, W. F.; Bürgi, R.; Peter, C.; Daura, X. *Angew. Chem., Int. Ed.* **2001**, *40*, 351−355.

(42) Daura, X.; Glättli, A.; Gee, P.; Peter, C.; van Gunsteren, W. F. *Adv. Protein Chem.* **2002**, *62*, 341−360.

(43) van Gunsteren, W. F.; Gattin, Z. Simulation of Folding Equilibria in Foldamers: Structure, Properties, and Applications. In *Simulation of Folding Equilibria in Foldamers: Structure, Properties, and Applications*; Hecht, S., Huc, I., Eds.; Wiley: Weinheim, Germany, 2007; pp 173−192.
(44) Daura, X.; Gademann, K.; Schäfer, H.; Jaun, B.; Seebach, D.; van Gunsteren, W. F. *J. Am. Chem. Soc.* **2001**, *123*, 2393−2404.
(45) Lin, Z. X.; Schmid, N.; van Gunsteren, W. F. *Mol. Phys.* **2011**, *109*, 493−506.
(46) Huang, W.; Lin, Z. X.; van Gunsteren, W. F. *J. Chem. Theory Comput.* **2011**, *7*, 1237−1243.
(47) Oostenbrink, C.; Villa, A.; Mark, A. E.; van Gunsteren, W. F. *J. Comput. Chem.* **2004**, *25*, 1656−1676.
(48) van Gunsteren, W. F. GROMOS. http://www.gromos.net (accessed March 21, 2014), the GROMOS software package and force fields can be downloaded from this Web site.
(49) Eichenberger, A. P.; Allison, J. R.; Dolenc, J.; Geerke, D. P.; Horta, B. A. C.; Meier, K.; Oostenbrink, C.; Schmid, N.; Steiner, D.; Wang, D. Q.; van Gunsteren, W. F. *J. Chem. Theory Comput.* **2011**, *7*, 3379−3390.
(50) Schmid, N.; Christ, C. D.; Christen, M.; Eichenberger, A. P.; van Gunsteren, W. F. *Comput. Phys. Commun.* **2012**, *183*, 890−903.
(51) Kunz, A. P. E.; Allison, J. R.; Geerke, D. P.; Horta, B. A. C.; Hünenberger, P. H.; Riniker, S.; Schmid, N.; van Gunsteren, W. F. *J. Comput. Chem.* **2012**, *33*, 340−353.
(52) Berendsen, H. J. C.; Postma, J. P. M.; van Gunsteren, W. F.; Dinola, A.; Haak, J. R. *J. Chem. Phys.* **1984**, *81*, 3684−3690.
(53) Tironi, I. G.; Sperb, R.; Smith, P. E.; van Gunsteren, W. F. *J. Chem. Phys.* **1995**, *102*, 5451−5459.
(54) *CRC Handbook of Chemistry and Physics*, 56th ed.; West, R. C., Ed.; CRC Press: Boca Raton, FL, 1976.
(55) Ryckaert, J. P.; Ciccotti, G.; Berendsen, H. J. C. *J. Comput. Phys.* **1977**, *23*, 327−341.
(56) Riniker, S.; Kunz, A. P. E.; van Gunsteren, W. F. *J. Chem. Theory Comput.* **2011**, *7*, 1469−1475.
(57) Christen, M.; Hünenberger, P. H.; Bakowies, D.; Baron, R.; Bürgi, R.; Geerke, D. P.; Heinz, T. N.; Kästenholz, M. A.; Kräutler, V.; Oostenbrink, C.; Peter, C.; Trzesniak, D.; van Gunsteren, W. F. *J. Comput. Chem.* **2005**, *26*, 1719−1751.
(58) Lin, Z.; van Gunsteren, W. F. *J. Comput. Chem.* **2013**, *34*, 2796−2805.
(59) Walser, R.; Mark, A. E.; van Gunsteren, W. F.; Lauterbach, M.; Wipff, G. *J. Chem. Phys.* **2000**, *112*, 10450−10459.
(60) Fraternali, F.; van Gunsteren, W. F. *J. Mol. Biol.* **1996**, *256*, 939−948.
(61) van Gunsteren, W. F.; Billeter, S. R.; Eising, A. A.; Hünenberger, P. H.; Krüger, P.; Mark, A. E.; Scott, W. R. P.; Tironi, I. G. *Biomolecular Simulation: The GROMOS96 Manual and User Guide*; Vdf Hochschulverlag AG an der ETH Zürich: Zürich, Switzerland, 1996.
(62) Wüthrich, K.; Billeter, M.; Braun, W. *J. Mol. Biol.* **1983**, *169*, 949−961.
(63) Steiner, D.; Allison, J. R.; Eichenberger, A. P.; van Gunsteren, W. F. *J. Biomol. NMR* **2012**, *53*, 223−246.
(64) *CRC Handbook of Chemistry and Physics*, 94th ed.; Haynes, W. M., Ed.; CRC Press: Boca Raton, FL, 2013.
(65) Daura, X.; Gademann, K.; Jaun, B.; Seebach, D.; van Gunsteren, W. F.; Mark, A. E. *Angew. Chem., Int. Ed.* **1999**, *38*, 236−240.
(66) Hurle, R. L.; Woolf, L. A. *Aust. J. Chem.* **1980**, *33*, 1947−1952.
(67) Seebach, D.; Ciceri, P. E.; Overhand, M.; Jaun, B.; Rigo, D.; Oberer, L.; Hommel, U.; Amstutz, R.; Widmer, H. *Helv. Chim. Acta* **1996**, *79*, 2043−2066.
(68) Seebach, D.; Abele, S.; Gademann, K.; Guichard, G.; Hintermann, T.; Jaun, B.; Matthews, J. L.; Schreiber, J. V. *Helv. Chim. Acta* **1998**, *81*, 932−982.